Energy 124 (2017) 214–226

Contents lists available at ScienceDirect

Energy

journal homepage: www.elsevier.com/locate/energy

Performance and emissions of a direct injection internal combustion engine devised for joint operation with a high-pressure thermochemical recuperation system

A. Poran, L. Tartakovsky*

Technion – Israel Institute of Technology, Technion City, Haifa 3200003, Israel

ARTICLE INFO

Article history:
Received 11 September 2016
Received in revised form
7 December 2016
Accepted 13 February 2017

Keywords:
Thermo-chemical recuperation
Steam reforming of methanol
Ethanol decomposition
High-pressure reforming
Reformate direct injection
Combustion of hydrogen-rich reformate

ABSTRACT

This paper presents the results of an experimental study on performance and pollutant emissions of a direct-injection spark-ignition engine devised for joint operation with a high-pressure thermochemical recuperation system based on methanol steam reforming. A comparison with gasoline and ethanol decomposition is performed. Engine feeding with methanol steam reforming products shows an 18%–39% increase in the indicated efficiency and a reduction of 73–94%, 90–96%, 85–97%, and 10–25% in NO_x, CO, HC and CO_2 emissions, respectively, compared to gasoline within a wide power range. Efficiency improvement and emissions reductions are obtained compared to ethanol decomposition products as well. The possibility of an unthrottled engine operating with a substantially lower cycle-to-cycle variation compared to both gasoline and ethanol decomposition is demonstrated. At high loads, the injector flow area was insufficient for a low injection pressure of 40 bar, leading to late injection and reduced engine efficiency for methanol steam reforming products. In the case of ethanol decomposition, the problem was less severe due to the higher energy content of ethanol decomposition products per mole. The concept of a direct-injection internal combustion engine with high-pressure methanol steam reforming shows good potential, while additional research on injection strategies and gaseous reformate combustion is required.

1. Introduction

In recent decades, there has been a continuous effort to reduce global environmental pollution and fossil oil consumption. As the main power source for transportation, internal combustion engines (ICE) are a major source of both environmental pollution and oil consumption. Thus, the reduction of pollutant and greenhouse gas (GHG) emissions generation as well as petroleum depletion can be achieved by increasing the ICEs' efficiency and using alternative low-carbon-intensity fuels. Ethanol and especially methanol are low-carbon-intensity fuels that are considered by many as good alternatives to petroleum because of their availability from various sources such as bio-mass, coal, natural gas and renewable energy-derived hydrogen [1–4]. In this article, we consider using these alcohols as the primary fuel in an ICE-reformer system with waste heat recovery (WHR) through high-pressure thermochemical recuperation (TCR).

It is known that in ICE, approximately 1/3 of the energy introduced with the fuel is wasted along with the hot exhaust gases [5]. Thus, partial utilization of this energy, also known as waste heat recovery, can lead to a significant increase in the overall ICE efficiency [6]. One possible method of WHR is utilizing the energy of hot exhaust gases to sustain endothermic fuel reforming reactions. This method is known as thermochemical recuperation [7]. TCR has two main benefits. First, it increases the fuel's LHV due to the WHR process through endothermic fuel reforming reactions — see Eqs. (1)–(3). Second, the mixture of gaseous reforming products (reformate) usually has a high hydrogen content, resulting in the increased burning velocity, higher octane number and wider flammability limits [8,9]. Thus, TCR allows improvement in the ICE efficiency, not only due to the WHR process but also lean-burn operating possibilities, which approach the theoretical Otto cycle and the possibility of increasing the engine compression ratio.

Aside from their previously mentioned advantages, methanol and ethanol are also excellent primary fuels for reforming since they can be reformed at relatively low temperatures

* Corresponding author.
E-mail address: tartak@technion.ac.il (L. Tartakovsky).

http://dx.doi.org/10.1016/j.energy.2017.02.074
0360-5442/

Nomenclature

Symbols

δR	uncertainty of calculated parameter R
δX_i	accuracy of measured value X_i
ΔH	enthalpy of reaction
e_b	burned zone energy
e_s	sensible energy
e_u	unburned zone energy
E_i	emissions of pollutant i
h_a	air enthalpy
h_{av}	enthalpy available for reforming
h_f	fuel enthalpy
$h_{f,i}$	injected fuel enthalpy
m	in-cylinder mass
m_a	air mass
$\dot{m}_a$	air flow rate
m_b	burned zone mass
m_f	fuel mass
$\dot{m}_f$	fuel flow rate
$m_{f,i}$	injected fuel mass
m_u	unburned zone mass
$\dot{m}_f$	fuel mass flow rate
M_C	molecular weight of carbon
M_i	molecular weight of pollutant i
p	cylinder pressure
Q	heat transfer rate
Q_b	burned zone heat transfer rate
Q_u	unburned zone heat transfer rate
V	cylinder volume
V_b	burned zone volume
V_d	displaced volume
V_u	unburned zone volume
$W_{i,g}$	gross indicated work
$\dot{W}_{i,g}$	gross indicated power
x_i	mass fraction of species i
$y_{c,fuel}$	fuel's carbon mass fraction
y_i	molar fraction of pollutant i
y_j	$CO/CO_2/CH_{1.85}$ molar fraction

Greek symbols

η_c	combustion efficiency
η_i	gross indicated efficiency
θ	crank angle (360 firing top dead center)
θ_{50}	anchor angle, the CAD of 50% fuel mass burned
θ_{0-10}	flame development angle, CAD difference ignition and 10% of the fuel mass is burned
θ_{10-75}	CAD difference between 10% and 75% of the fuel mass burned
θ_{10-90}	rapid burning angle – CAD difference between 10% and 90% of the fuel mass burned
λ	excess air ratio
σ_{IMEP}	IMEP standard deviation

Acronyms

BTE	brake thermal efficiency
CAD	crank angle degrees
COV	coefficient of variation in the IMEP
DI	direct injection
ED	ethanol decomposition
HC	hydrocarbons
HRR	heat release rate
ICE	internal combustion engine
IMEP	indicated mean effective pressure (gross)
LHV	lower heating value
MD	methanol decomposition
MSR	methanol steam reforming
PN	particle number concentration
SI	spark ignition
TCR	thermochemical recuperation
TDC	top dead center
WHR	waste heat recovery
WOT	wide-open throttle

(approximately 250–300 °C [3,10]) to produce hydrogen-rich reformate. Commonly investigated reforming reactions for ICE applications are methanol decomposition — MD (Eq. (1)), methanol steam reforming — MSR (Eq. (2)), and low-temperature ethanol decomposition — ED (Eq. (3)) [11–13].

$$CH_3OH_{(g)} \rightarrow CO + 2H_2 \quad \Delta H = 90 \text{ kJ/mol} \tag{1}$$

$$CH_3OH_{(g)} + H_2O_{(g)} \rightarrow CO_2 + 3H_2 \quad \Delta H = 50 \text{ kJ/mol} \tag{2}$$

$$C_2H_5OH_{(g)} \rightarrow CH_4 + CO + H_2 \quad \Delta H = 50 \text{ kJ/mol} \tag{3}$$

In this work, we focused mainly on MSR and ED due to the problems of catalyst stability and deactivation that are frequently observed in the MD process [14,15]. It is possible that newly developed catalysts will make MD a beneficial option in the future [16].

Methanol reforming schemes investigated in the past showed up to 40% brake thermal efficiency (BTE) improvement compared to their gasoline counterparts but have also exhibited serious problems [17]. The main problems reported include uncontrolled combustion, catalyst deactivation, cold start and engine maximal power loss due to reduced volumetric efficiency. The latter is a result of supplying gaseous reformate into the intake system that reduces the partial pressure of the air in the intake manifold, and the absence of an evaporative cooling effect compared to the case of a liquid fuel port injection.

More recent studies have reported on a high-efficiency, low-emission hydrogen-fueled ICE, for which the problems of reduced power and uncontrolled combustion were solved by the direct injection (DI) of hydrogen [18]. Hagos et al. [19,20] studied the combustion of syngas ($H_2 + CO$) derived from biomass gasification in a DI SI engine and reported on the possibility of CO and HC emissions reduction together with NO_x emissions increases at higher loads. Li et al. [21] and Shimada & Ishikawa [22] studied the onboard reforming of hydrous ethanol with a reformate supply to the intake manifold. Both reformate gas and unreformed ethanol were burned for power production. They reported on engine efficiency improvement up to 18%, together with a substantial decrease in NO_x, CO and THC emissions. Yoon [23] studied reformer design limitations for the steam reforming of methanol. He [24] proved that H_2 and CO participation in the combustion process of ICE results in the increase of O, H and OH radicals' concentration and hence improves the flame propagation and combustion process. Recent studies propose solving the cold start problem by integrating the reforming system in an electric-hybrid vehicle and

keeping a small on-board pressurized vessel with reformate for start-up or injection of some of the primary fuel with a port fuel injector [20,25]. In a previous study [26], we suggested the high-pressure TCR concept and showed that performing the reforming reactions at high pressure is essential to enabling direct injection of the reformate. Otherwise, a significant fraction of the engine power would be required to compress the reformate prior to its injection [26]. In Ref. [27], Peppley showed that a commercial CuO/ZnO/Al_2O_3 catalyst was able to support MSR reactions without a significant deactivation problem up to a pressure of 40 bar. Since no evidence of catalyst stability at high-pressure MD was reported, we focused our research on MSR. Assuming that an MD catalyst will prove to be stable at high pressures, this reaction may be beneficial because there will be no need to carry, preheat and evaporate water in the reformer; the reformate heating value will be greater; and lower injection pressure will be required. An advantage of MSR over MD is that the presence of CO_2 in the reformate greatly contributes to the decrease of the in-cylinder temperature and thus leads to the reduction of NO_x formation.

In a previous article [26], we conducted a simulation of ICE with a high-pressure TCR system based on methanol steam reforming and showed that the BTE improvement of 14% can be achieved at a rated power regime compared to the gasoline-fed counterpart. Previous simulations also showed that engine feeding with MSR and ED products results in reduced pollutant emissions compared to gasoline [25]. BTE — in the case of ICE feeding with MSR products — was predicted to be higher compared to ED and gasoline [25]. The research reported in this article aimed at an experimental proof of previous theoretical findings and demonstrated that a DI SI ICE fed by MSR reforming products can efficiently operate at an injection pressure proven to be feasible for high-pressure TCR as a milestone to creating a complete system of ICE with high-pressure thermochemical recuperation.

2. Methodology

2.1. Experimental setup

The experimental setup is based on a single-cylinder, direct-injection SI engine designed to operate with the direct injection of various gaseous fuels such as MSR, ED, methane etc., as well as a carburetor gasoline-fed engine (baseline configuration). The engine was built as a part of the laboratory system of ICE with high-pressure TCR aimed at proving the feasibility of the system. Fig. 1 shows a schematic of the experimental setup.

The laboratory engine was based on a Robin-EY20-3 4-stroke spark ignition (SI) air-cooled, single cylinder ICE (1) coupled with a Sincro GP100 2.2 kW AC 230 V generator (13). This engine was selected as the basis for the first prototype of a DI MSR-fed engine because of the extra space in the cylinder head that enabled the relatively easy addition of a gas-DI injector and a pressure transducer. The main parameters of the baseline engine are listed in Table 1.

The original ICE ignition system was replaced by an AEM 30-2853 coil (2) and a Denso IWF 24 Iridium spark plug (3) to enable a spark charge and spark timing variation.

Engine control and data logging were carried out with a dSPACE DS 1104 controller board (9) connected to a computer (34). In-cylinder pressure and crank angle measurements for a combustion process analysis were performed with a Kistler crankshaft encoder 2613B (7) at a resolution of 0.5° mounted on the free end of the generator shaft; a Kistler 6061B water-cooled pressure transducer (5) and a Kistler 5018 charge amplifier (6). The pressure transducer was installed in the cylinder head according to the manufacturer instructions.

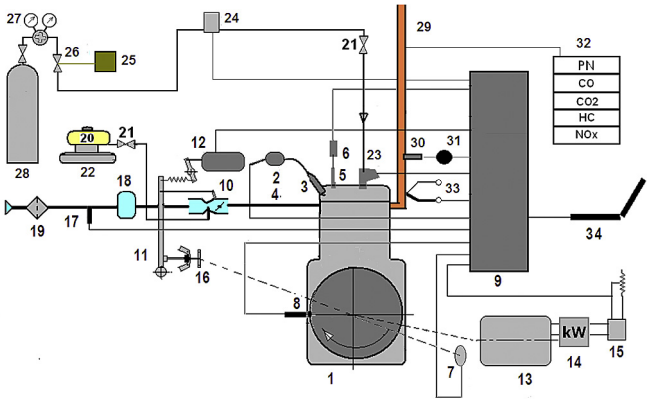

Fig. 1. Schematic of the experimental setup. 1 - Robin EY20-3 single cylinder ICE; 2 - ignition coil; 3 - spark plug; 4 - air intake system; 5 - pressure transducer; 6 - charge amplifier; 7 - crankshaft encoder; 8 - TDC proximity sensor; 9 - data acquisitor and controller; 10 – throttle; 11 – centrifugal speed governor; 12 – linear actuator; 13 – generator; 14 – power gauge 15 – trace driven generator load; 16 – crankshaft driven gear of the engine speed governor; 17 – air flow meter; 18 – pressure wave damper; 19 – air filter; 20 – gasoline tank; 21 – valve; 22 – electronic scales; 23 - DI gas injector; 24 – gas flow meter; 25 – hydrogen detector; 26 – emergency self-acting stop cock; 27 – pressure regulator; 28 – gas cylinder; 29 – exhaust line; 30 – O_2 sensor; 31 – air to fuel ratio gauge; 32 – exhaust gas analyzers; 33 – thermocouple; 34 - computer.

Table 1
Specifications of Robin EY-20 ICE.

Bore x Stroke, mm	67 × 52
Displacement, cm^3	183
Compression ratio	6.3
Power, kW @ speed, rpm	2.2 @ 3000
Continues BMEP @ 3000 rpm, bar	4.8
Gasoline feed system	Carburetor

The desired engine speed was regulated by varying the spring load of the governor with a linear actuator (12) in the case of gasoline-fed operating and by changing the quantity of the injected fuel and load for the case of gaseous wide-open-throttle (WOT) operation. The engine load was controlled via resistors and a rheostat, which were connected to the gen-set generator.

The gaseous fuel flow was measured by a Bronkhorst F111-AI-70K-ABD-55-E mass flowmeter (24). Conversion between various gas types was performed using FLUIDAT software based on the constant pressure heat capacities of the mixtures. Gasoline consumption was measured using the digital scales GF-12K from A&D Ltd. (22).

Gaseous fuels were supplied to the engine from premixed compressed gas vessels (28) with a mix accuracy of 1% of the lowest concentration species that was provided by a supplier of gas mixtures. The desired injection pressure was set by a pressure regulator.

The CO_2 and CO concentrations were measured from a dried exhaust gas sample line with a California Analytical Instrument (CAI) 600 series NDIR analyzer. The NO_x was measured from the same sampling line using a Thermal Converter 501x and NO_x chemiluminescent analyzer 200 EH from Teledyne Instruments. Total hydrocarbons (HC) were measured directly from the exhaust line with a CAI 600 series FID HC analyzer. The nanoparticle number concentration (PN) and size distribution were measured with an Engine Exhaust Particle Sizer 3090 (EEPS) equipped with a 379020A rotating disk thermodiluter; both are produced by TSI (32).

The intake air flow was measured by a VA-420 flow sensor and

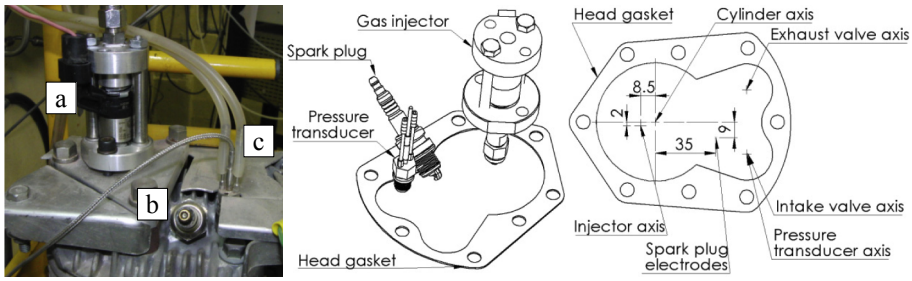

Fig. 2. On the left: a picture of the gas injector (a) spark plug (b) and pressure transducer (c) as installed on the cylinder head. In the middle: a drawing of the same components' orientation with the cylinder head omitted to enable a clear view of the components. On the right: the relative location of the spark plug, injector and pressure transducer (dimensions are shown in mm). The spark plug electrodes and injector nozzle are located 12 mm and 0.3 mm above the gasket plane, respectively.

was verified by the calculation of an exhaust gas carbon balance and by using a wide-band Lambda sensor kit LC-1 from Innovate Motorsports, which was based on a Bosch LSU 4.2 O_2 sensor (30).

In the research, we used an in-house-developed direct gaseous fuel injector. The injector was developed based on a commercial Magneti Marelli IHP072 gasoline DI injector. The modification was made to the nozzle to allow higher volumetric flow rates required for gaseous fuel injection. The flow diameter of the injector was 0.85 mm^2, and its discharge coefficient was in the range of 0.87± 0.07. Further details regarding the injector can be found in Ref. [28]. The relative location of the injector, spark plug and pressure transducer can be seen in Fig. 2. The optimization of the location and orientation of the gas DI injector was beyond the scope of this work and is not discussed hereinafter.

The ignition timing for each fuel was constant and set as the MBT value for the specified speed at WOT and the mid-range of the air excess factor: for MSR, @ $\lambda = 2$; for ED, @ $\lambda = 1.5$; and for gasoline, @ $\lambda = 1$. Obtaining the MBT ignition timing values for each studied engine operating mode was not possible due to limited amount of available MSR and ED gases.

2.2. Data processing

The measured data were processed to obtain the results as described in the following section.

The gross indicated mean effective pressure (IMEP) is defined following Eq. (4):

$$IMEP = \frac{\int pdV}{V_d} = \frac{W_{i,g}}{V_d} \tag{4}$$

where V_d is the displaced volume; V is the cylinder volume; p is the cylinder pressure; and $W_{i,g}$ is the gross indicated work.

The IMEP was calculated by integrating the in-cylinder pressure values over the cylinder volume for the compression and expansion strokes only (gross). The integration was performed numerically using the trapezoidal method. For every engine regime shown in this work, approximately 100 cycles were measured, and the IMEP shown is that of the average cycle for the considered regime. An important parameter of the engine is the IMEP coefficient of variation (COV). It is defined as the standard deviation of the IMEP divided by the mean IMEP (Eq. (5)) [30]:

$$COV = \frac{\sigma_{IMEP}}{IMEP} \tag{5}$$

where σ_{IMEP} is the IMEP standard deviation and IMEP is the average IMEP of all cycles.

The gross indicated efficiency (η_i) was calculated following Eq. (6) [30]:

$$\eta_i = \frac{W_{i,g}}{m_f \cdot LHV_f} \tag{6}$$

where m_f is the fuel mass supplied to the cylinder per cycle and LHV_f is the lower heating value of the fuel.

For the case of reforming products, the indicated efficiency was calculated based on the primary fuel mass that is required to produce the reforming products and the primary fuel's LHV. For example, the indicated efficiency for the MSR products was calculated according to Eq. (7).

$$\eta_{MSR} = \frac{W_{i,g}}{\frac{n_M \cdot M_M}{n_W \cdot M_W + n_M \cdot M_M} \cdot m_{MSR} \cdot LHV_M} \tag{7}$$

where $W_{i,g}$ is the gross indicated work; m_{MSR} is the MSR products mass supplied to the cylinder per cycle; n_M is the number of methanol moles participating in the MSR reaction; n_W is the number of water moles participating in the MSR reaction; M_M is the molar mass of the methanol; M_W is the molar mass of water; and LHV_M is the lower heating value of the methanol.

The burned mass fraction and heat release rate (HRR) results were obtained by processing the measured values of the in-cylinder pressure and piston position using GT-Power software. Pressure pegging was performed using the least squares method as described in Ref. [31]. Because the injection of gaseous fuel started soon after the inlet valve close, in these cases, the method was applied for the compression period after the end of the injection and before the ignition. Moreover, all pegging results were double-checked using another method, where the error between the measured and simulated (using GT-Power) pressure values during 40 CAD after the intake valve closing in the compression stroke is minimized by applying a pressure offset shift. An advantage of this approach is that it uses extra measured values, such as fuel mass and fresh air contents in the cylinder. Both methods produced similar results in the considered range of engine operating modes. A two-zone combustion methodology was used by applying the first law for control volume — Eqs. (8) and (9) [32].

$$\frac{d(m_u e_u)}{dt} = -p\frac{dV_u}{dt} - Q_u + \left(\frac{dm_f}{dt}h_f + \frac{dm_a}{dt}h_a\right) + \frac{dm_{f,i}}{dt}h_{f,i} \tag{8}$$

$$\frac{d(m_b e_b)}{dt} = -p\frac{dV_b}{dt} - Q_b - \left(\frac{dm_f}{dt}h_f + \frac{dm_a}{dt}h_a\right) \tag{9}$$

where m_u is the unburned zone mass; e_u is the unburned zone energy; p is the in-cylinder pressure; V_u is the unburned zone volume; Q_u is the unburned zone heat transfer rate; m_f is the fuel

mass; h_f is the fuel enthalpy; m_a is the air mass; h_a is the air enthalpy; $m_{f,i}$ is the injected fuel mass; $h_{f,i}$ is the injected fuel enthalpy; m_b is the burned zone mass; e_b is the burned zone energy; V_b is the burned zone volume; and Q_b is the burned zone heat transfer rate.

Following the applied two-zone model, at the beginning of the combustion, the entire cylinder content is in the unburned zone, and at any time step, a certain amount of unburned mixture is transferred to the burned zone. In the burned zone, the equilibrium of 11 possible combustion products is assumed; thus, the temperature and pressure are obtained. Iterations for the amount of unburned mixture that transferred to the burned zone are made until the obtained pressure matches the measured pressure. Additional information that was required for the burned mass fraction calculation is the heat transfer to the cylinder walls and a residual gas fraction in the cylinder. The heat transfer was calculated using the Woschni engine model without swirl or tumble. A convection heat transfer multiplier was applied to match the measured pressure results and measured exhaust gas temperatures assuming that 100% of the fuel mass is burned. The residual gas fraction was calculated by creating an engine model in GT-Power software and calibrating it to the measured results, and then re-applying the residual gas fraction to the combustion analysis. Based on the obtained instantaneous values of the burned mass fraction, the following parameters were calculated and analyzed: flame development angleθ_{0-10}, rapid burning angle θ_{10-90} and θ_{10-75}− CAD difference between 10% and 75% of the fuel mass burned.

The heat release rate was calculated using the same assumptions but with a single-zone first law Eq. (10) for control volume [30].

$$HRR = -p\frac{dV}{d\theta} - Q - \frac{d(m\cdot e_s)}{d\theta} \tag{10}$$

where V is the cylinder volume; θ is the crank angle; Q is the heat transfer rate; m is the in-cylinder mass; and e_s is the sensible energy of the cylinder content.

The maximum pressure was calculated for the averaged and filtered engine cycle for each operating mode. The available exhaust enthalpy was calculated based on the measured fuel flow rate, air-to-fuel ratio and exhaust gas temperature assuming an ideal gas mixture and the exhaust gas composition of complete fuel combustion for specific heat calculations. The reference state for enthalpy availability was chosen as 200 °C. This reference temperature was chosen to provide a sufficient temperature gradient for a heat exchange between the exhaust gases and the primary fuel that is expected to enter the reformer after preheating it at approximately 150 °C.

The combustion efficiency η_c was calculated according to Eq. (11) [30]:

$$\eta_c = 1 - \frac{\left(\dot{m}_a + \dot{m}_f\right)\left(\sum_i x_i \cdot LHV_i\right)}{\dot{m}_f \cdot LHV_f} \tag{11}$$

where $\dot{m}_f$ is the fuel flow rate; $\dot{m}_a$ is the air flow rate; x_i is the mass fraction of species i; LHV_i is the LHV of species i; and LHV_f is LHV of the fuel.

The heating value of 44 kJ/kg was assumed for HC. The hydrogen content in the exhaust gases was not measured and was thus omitted from the calculation, which introduces some upward bias in the obtained values of combustion efficiency.

A conversion of the measured pollutant concentrations to specific pollutant emissions (in g/kWh) was performed based on a carbon balance analysis, measured fuel flow rates and the assumption that the lube oil burn and particulate formation effects on the carbon balance are negligible (Eq. (12)).

$$E_i = \frac{\dot{m}_f \cdot y_{c,fuel} \cdot y_i \cdot M_i}{M_C \cdot \sum y_j \cdot \dot{W}_{i,g}} \tag{12}$$

whereE_i is the specific pollutant emission of pollutant i; $\dot{m}_f$ is the fuel mass flow rate; $y_{c,fuel}$ is the fuel's carbon mass fraction; y_i is the molar fraction of pollutant i; M_i is the molecular weight of pollutant i; M_C is the molecular weight of carbon; y_j is the $CO/CO_2/CH_{1.85}$ molar fraction; and $\dot{W}_{i,g}$ is the gross indicated power.

The uncertainty of the calculated parameters was assessed using Eq. (13) [33]:

Table 2
Accuracy of measured data and uncertainty of calculated parameters.

Accuracy of measured parameters	
Device	Manufacturer, (Accuracy)
Crankshaft encoder 2613B	Kistler Instrument A.G., (Resolution 0.5°, Dynamic accuracy +0.02° at 10000 rpm)
Charge Amplifier Type 5018	Kistler Instrument A.G., (<±0.3% at 0–60 °C)
Water cooled pressure transducer 6061B	Kistler Instrument A.G., (Max. linearity ≤±0.29% FS[a])
Mass flow meter F111-AI-70K-ABD-55-E	Bronkhorst High-Tech B.V., ±(0.5% of MV[a]+0.1% of FS[a])
Air flow sensor VA420 with integrated measuring unit	CS Instruments GmbH, (±1.5% of MV[a])
Wide-band Lambda sensor LC-1 kit	Innovate Motorsports based on Bosch LSU 4.2 O_2 sensor, (at λ = 1: ±0.007; at λ = 1.7: ±0.05)
NO_x analyzer 200 EH	Teledyne Instruments, (0.5% of MV[a])
HC analyzer 600 series	California Analytical Instruments, (±0.5% of FS[a])
CO, CO_2 analyzer 600 series	California Analytical Instruments, (±1% of FS[a])
Exhaust Engine Particle Sizer 3090	TSI, NA[a,b]
Rotating Disk Thermodiluter 379020A	TSI, (±10%)
Power gauge (Wattmeter) DW-6060	Lutron Electronics Company, (±1%)
Digital scales GF-12K	A&D Ltd, (±0.1 g)
Maximal uncertainty of calculated parameters	
IMEP	±5%
Indicated Power	±5%
COV	±4%

[a] FS – full scale, MV – Measured value, NA – Not available.
[b] It was found in Ref. [29] that the new SOOT matrix recently developed by TSI to improve the EEPS PN concentration and size distribution measuring accuracy (which was used in our study) provides PN concentration readings in the range of 84%–96% of those obtained with a scanning mobility particle sizer (SMPS) across a wide range of diesel engine operating conditions.

$$\delta R = \left(\sum_{i=1}^{N} \left(\frac{\partial R}{\partial X_i} \delta X_i \right)^2 \right)^{1/2} \quad (13)$$

where δR is the uncertainty of calculated parameter R; $\frac{\partial R}{\partial X_i}$ is the partial derivative of R with respect to measured valueX_i; and δX_i is the accuracy of measured valueX_i.

It is known that the IMEP calculation is insensitive to random noise and absolute pressure referencing errors but is very sensitive to crank phasing errors [34]. The calculation also involves numerical integration. Thus, COV and IMEP uncertainty were calculated by applying the approach suggested by Moffat [33] for computing uncertainty when a computer program is used for the results analysis. An angle phase error of ±0.5° was used in this calculation (equal to the encoder resolution). The average IMEP error was found to be 2.5% with a maximal error of 5% that was observed at idle and engine feeding with a gaseous fuel. Table 2 summarizes the accuracy of the measured data and uncertainty of the calculated parameters. The uncertainty values calculated for COV; indicated efficiency, combustion efficiency; and NO_x, HC, CO and CO_2 emissions are shown as error bars in Figs. 3 and 6-11. The uncertainty values are shown for all measurement results presented in Figs. 3 and 6-11. However, in some cases, due to the wide range of values shown in one graph, error bars may not be seen due to their relatively small absolute values.

3. Results and discussion

This section consists of two main parts. The first part discusses the reformates' influence on the combustion process in an ICE and provides a comparison with gasoline and methane. The second part discusses the effects of engine feeding by reforming products based on its performance in terms of the indicated efficiency and pollutant emissions.

3.1. Combustion process

Cycle-to-cycle variation is an important parameter indicating the quality of the combustion process for two main reasons. First, the optimum spark timing is normally set for an average cycle. Thus, for a fast burning cycle, the ignition is actually over-advanced, and for a slow burning cycle, it is over-retarded. This results in the loss of power and efficiency. Second, fast burning cycles lead to high in-cylinder pressure, high pressure rise rates, and high NO_x formation and may also lead to knock appearance. These fast cycles limit the engine's compression ratio and affect the possibility of tuning optimization [30]. Cyclic variations in the cylinder are caused by a mixture motion variation, especially in the vicinity of the spark plug because they change the early flame development and thus affect the fuel burning behavior and the heat release rate. The fuel burning velocity has significant influence on the cycle-to-cycle variability since it influences the early flame development and thus affects the overall heat release rate. The higher burning velocity of a fuel-air mixture reduces the cyclic variations and hence has a beneficial effect on engine efficiency and emissions. Fig. 3 shows the COV of MSR and ED as function of λ at constant ignition timing and WOT compared to the reference cases of gasoline and methane.

As expected, the COV for ED and MSR was substantially lower than in the cases of engine feeding with gasoline and methane thanks to the presence of hydrogen in the reformate that increases the mixture laminar burning velocity [35]. Moreover, the COV values in the cases of engine feeding with reforming products do not exceed 0.05 up to $\lambda = 3.5$ and $\lambda = 2$ for MSR and ED, respectively. COV $\leq$0.05 is widely accepted as a sign of stable, well-tuned engine operation [2]. Thus, in the case of ICE feeding with reformates, efficient operation is possible at very lean fuel-air mixtures, especially for MSR reformate fuel. The MSR reformate allows stable operation for a wider range than ED due to the higher molar fraction of hydrogen in the mixture (75% compared to 33.3%). It is important to underline that the ICE was able to work unthrottled with both MSR and ED reformates up to low idle. However, for ED, the COV at high idle reached an unacceptably high value of 0.37 due to the misfire appearance, which resulted in poor combustion efficiency and high HC emissions (Figs. 7 and 10). Thus, for this setup, unthrottled operation with ED in the entire load range was not

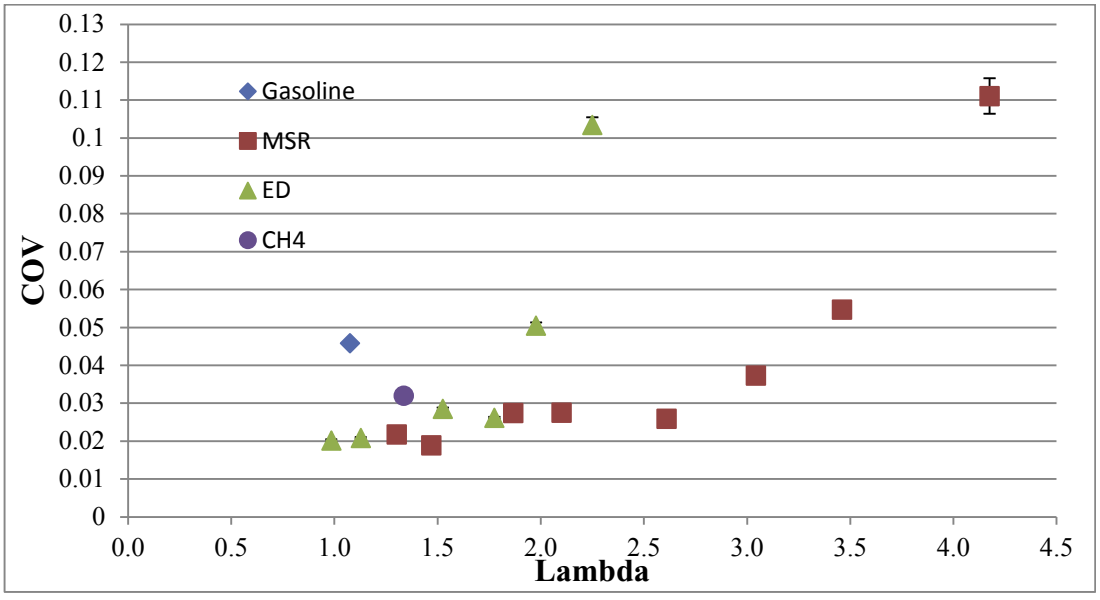

Fig. 3. Cycle-to-cycle variation as a function of Lambda for various fuels. Engine speed 2800 rpm; the MSR and ED operated at WOT, and the injection pressure was at 40 bar. The gasoline and methane were at IMEP 3.6 bar. The ignition timing for gasoline MSR and ED was constant at 333, 347 and 339 CAD, respectively. The error bars show the uncertainty of the calculated COV values.

recommended. However, this may not be true for an engine with a higher compression ratio, different injector nozzle, optimized spark timing for WOT idle, and a different injector and spark plug relative location. It should be noted that for MSR reformate, even with the negative influence of all of the above mentioned circumstances, the COV value at the WOT idle operating mode did not exceed 0.11.

The fuel burning velocity has also a significant effect on the heat release process. A high burning velocity leads to an increase of HRR. The latter results in thermal efficiency improvement because the engine working cycle approaches the theoretical Otto cycle. However, at the same time, the maximal in-cylinder pressure, pressure rise rate and heat transfer losses increase due to higher in-cylinder temperatures. An example of a few typical HRR curves for the different fuels considered in this work is shown in Fig. 4.

As seen from Fig. 4, the HRR of MSR products is significantly higher than those of gasoline and methane, but can be moderated by increasing λ to a degree where their HRR is comparable. Since the brake power for all shown cases is the same, the highest brake thermal efficiency is achieved for the case where the least heat is released (i.e., the least area under the HRR-CAD graph). The highest BTE is obtained for engine feeding with MSR reformate at $\lambda = 2.6$. This is a result of the positive effect of reduced pumping and heat transfer losses that overcome the negative effect of lower HRR. At the considered engine operating mode (800 W @ 2800 rpm) in case of ICE feeding with MSR reformate, the highest efficiency is achieved at the highest possible λ. When power is kept constant, the maximal pressure p_{max} does not change substantially as the air-fuel ratio varies. For example, when λ changes from 1.2 to 2.6, the values of p_{max} change from 17.5 to 16.9 bar only. This is a result of two contradicting effects. The HRR decreases at higher air excess factors, thus aiming at maximal pressure reduction. At the same time, cylinder pressure at the start of compression increases with λ rise, as a result of throttle opening, thus acting toward the maximal pressure increase. Fig. 5 shows a comparison of flame development (θ_{0-10}) and rapid burning angle (θ_{10-90}) parameters for different fuels and air-fuel ratios.

The flame development angle (θ_{0-10}) for MSR products is much lower than those of methane, ED and gasoline – Fig. 5. This explains the lower COV of MSR at a wide range of excess air ratios. It can also be seen that in the case of MSR with $\lambda = 1.5$ and especially $\lambda = 1.2$, the rapid burning angle (θ_{10-90}) is much higher than expected. This is a result of the insufficient flow rate through the injector, which resulted in a longer injection duration (until 15 CAD after ignition) and thus led to late end of combustion and reduced combustion efficiency. The non-optimized injector positioning (a relatively large distance between the gas injector and the spark plug) also contributed to the retarded combustion of the portion of the fuel that was injected late. In the case of a higher mass flow rate through the injector, it is expected that the rapid burning angle may be further reduced because of the shorter injection duration, which enables more time for fuel-air mixing.

The exhaust gas temperature is also an important parameter when considering a TCR system since the exhaust energy is used for the fuel reforming. Although the temperature of the exhaust gas decreases as the air-to-fuel ratio increases, the exhaust mass flow rate increases (as a result of throttle opening) and heat transfer losses to the cylinder walls decrease. Thus, the reduction of available enthalpy (when it is considered as a percentage of the fuel's energy) with Lambda increase is quite moderate compared to the observed decrease in the exhaust gas temperature (Table 3). It is useful to consider the available enthalpy of exhaust gas as a percentage of the energy introduced to the engine with the fuel ($\dot{m}_f \cdot LHV_f$) since this enthalpy is used to reform the same fuel and flow rates of the fuel and the exhaust gas are interrelated. For the case of MSR with $\lambda = 1.2$, the enthalpy availability is exceptionally high due to the late end of injection that leads to fuel burning late in the expansion stroke (Figs. 4 and 5; Table 3).

3.2. Engine performance

As explained in the previous section, the beneficial properties of hydrogen-rich ED and MSR fuels, together with the WHR advantages, allow for much better efficiency, especially at low loads. Fig. 6 shows the engine-indicated efficiency when fed with the various fuels as a function of engine load (IMEP).

As seen from Fig. 6, the thermal efficiency of the engine fueled by MSR products was improved by 18–39% (relative) compared to the engine operating with gasoline. At higher loads (IMEP > 4 bar), there was an insufficient MSR reformate flow rate through the injector. This required late end of injection (up to 5 CAD before ignition) and along with a non-optimized positioning of the injector resulted in fuel combustion late in the expansion stroke (see Figs. 4 and 5) and, as a result, lower efficiency – Fig. 6. This problem can be resolved by increasing the injector flow area or

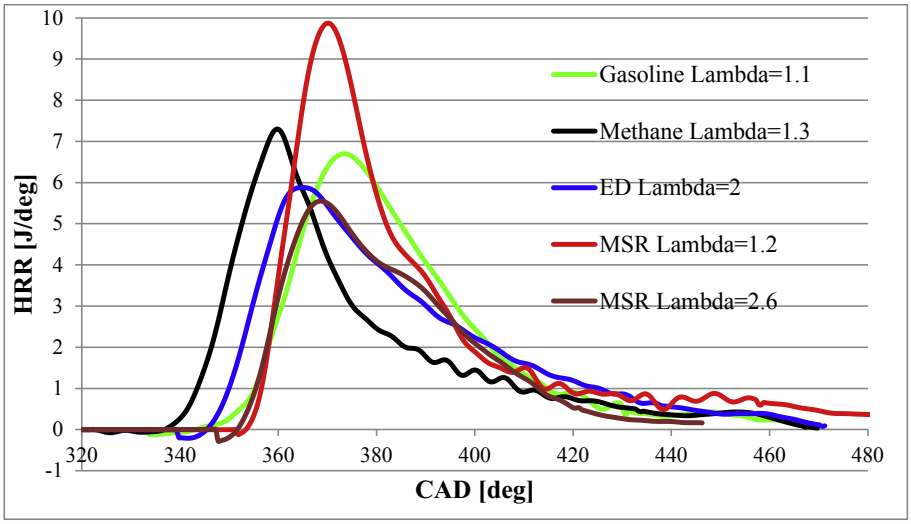

Fig. 4. Example of typical HRR for different fuels. Engine speed 2800 rpm; measured power 800 W; gas injection pressure, 40 bar.

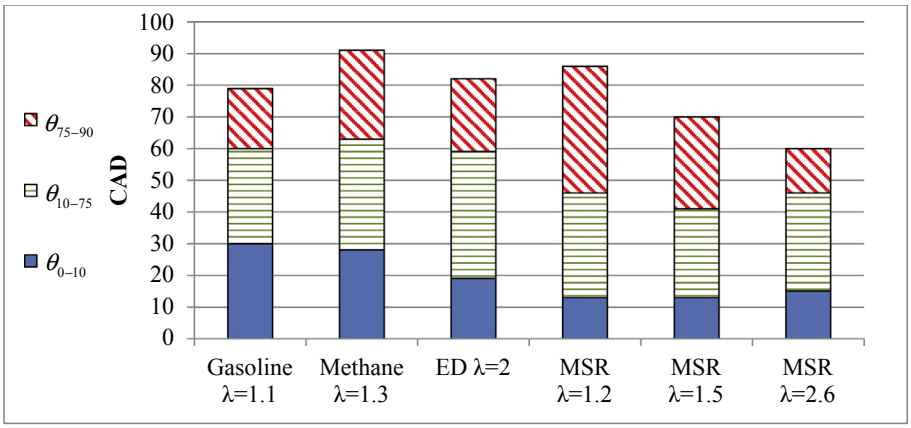

Fig. 5. Flame propagation angles for different fuels and air excess ratios. Engine speed 2800 rpm, measured power 800 W, injection pressure 40 bar; θ_{0-10} - flame development angle; θ_{10-75} – CAD difference between 10% and 75% of fuel mass burned; θ_{75-90}- CAD difference between 75% and 90% of fuel mass burned.

Table 3
Exhaust gas temperatures and available enthalpy for different fuels and A/F ratios, $\dot{W}_{i,g} = 1.5$ kW.

	Gasoline λ = 1.1	Methane λ = 1.3	ED λ = 2	MSR λ = 1.2	MSR λ = 1.5	MSR λ = 2.6
T_{exh} [°C]	583	454	450	634	502	396
h_{av} [kW]	1.03	0.8	1.11	1.68	1.17	0.88
Available enthalpy, % of fuel energy	16	14	19	22	18	18

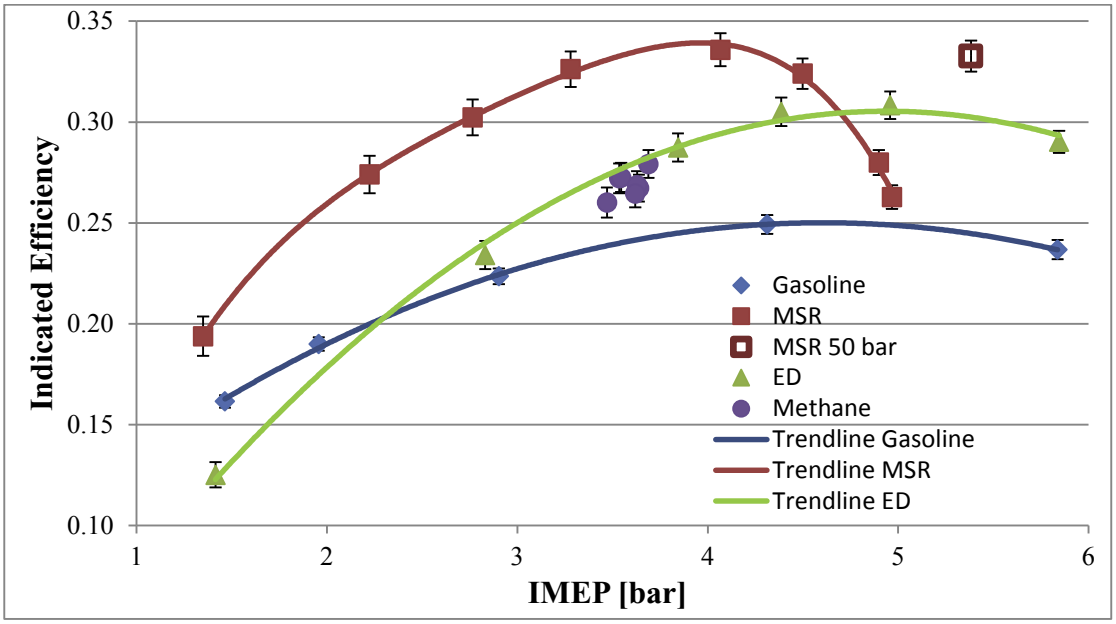

Fig. 6. Engine-indicated efficiency at various load regimes. Engine speed 2800 rpm; ED and MSR at WOT; injection pressure at 40 bar; injection start at 230 CAD. The ignition timing for gasoline, MSR and ED was constant at 333, 347 and 339 CAD, respectively. The error bars show uncertainty for the calculated indicated efficiency values.

injection pressure. In our case, the latter solution was easier, and by increasing the injection pressure up to 50 bar, we have achieved an indicated efficiency of 0.33 at an IMEP of 5.4 bar. Fig. 6 reveals that the reformate flow rate problem was less severe for the case of ED due to the higher energy density of the ED products compared to the MSR reformate. Although ED has this advantage over MSR, for most of the engine operating range, MSR showed superior efficiency. At low loads (close to idle), the indicated efficiency of the engine fed with MSR and ED reformates reduced rapidly, also because we worked at WOT, which led to high Lambda values and, as a result, high COV (Fig. 3) and non-optimized ignition timing for these regimes (which was constant throughout this experiment). In the case of engine feeding with ED, it also led to poor combustion efficiency (Fig. 7). This effect was less obvious for gasoline, where Lambda remained constant. However, when operating with the MSR reformate, the engine efficiency remained substantially higher compared to gasoline, even at the lowest engine loads.

Fig. 7 shows that even though it is possible to work unthrottled with the ED reformate up to idle, the combustion efficiency in this case decreases to unacceptably low values, which makes throttling

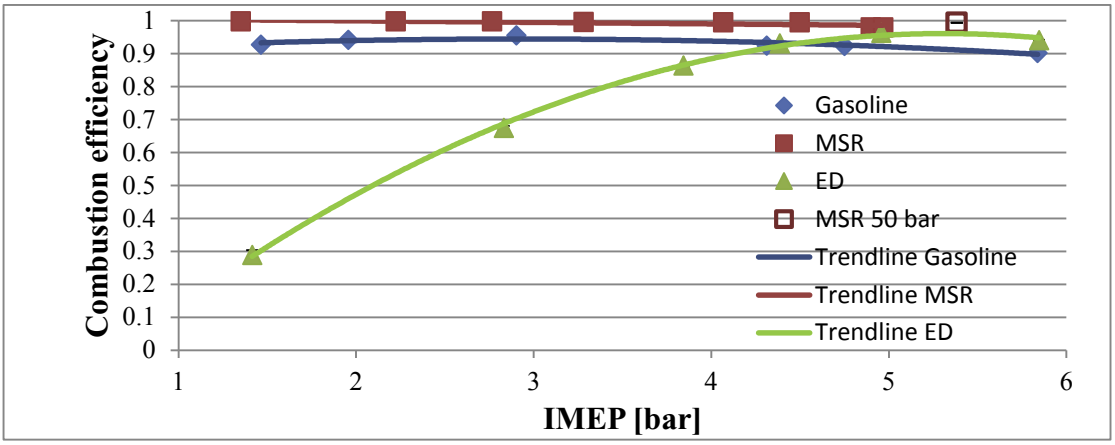

Fig. 7. Combustion efficiency at various load regimes. Engine speed 2800 rpm; ED and MSR at WOT; injection pressure at 40 bar; injection start at 230 CAD. The ignition timing for gasoline, MSR and ED was constant at 333, 347 and 339 CAD, respectively. The error bars show uncertainty in the calculated combustion efficiency values.

the beneficial option. It is expected that this problem would be less severe for higher compression ratio engines. For MSR, a reduction in combustion efficiency is not apparent because of the wider flammability limits of the hydrogen-rich mixture (the lack of H_2 content measurement in the exhaust gas can result in some overestimates of the calculated combustion efficiency values). The reduction in indicated efficiency for the case of engine feeding with MSR may be mainly attributed to the reasons offered earlier (high COV, non-optimal ignition timing). Throttling, to some extent, may also be beneficial for MSR at low loads because of the need to reduce cycle-to-cycle variability and to ensure the available enthalpy required for primary fuel reforming. However, the optimization of engine performance at low-load regimes, when operating with reformate fuel, was beyond the scope of this work.

One of the most important advantages of reformates over gasoline is the possibility of pollutant emissions mitigation due to the efficient combustion of low carbon intensity and hydrogen-rich gaseous fuel. Figs. 8–11 show a comparison of pollutant emissions between gasoline, ED and MSR reformates.

As expected, substantially lower NO_x emissions were measured for reformate fuels compared to those of gasoline-fed engines, which is due to the lean burn of reformates that allowed substantially lower maximal in-cylinder temperatures and, as a result, weaker NO_x formation. As the load increases and the mixture becomes richer, the NO_x formation process intensifies. However, in the case of engine feeding with MSR products, the fuel injected into the cylinder contains a substantial amount of CO_2 (it constitutes 17% wt. of a stoichiometric air-MSR fuel mixture). The latter works as an inherent EGR: reduces the in-cylinder temperatures and as a result leads to lower NO_x formation. The obtained results show that ICE operating with MSR products leads to a reduction of NO_x emissions by 73–94% in the entire tested range of engine loads.

The CO emissions of direct-injection SI ICE fed with MSR products remain lower than 5 g/kWh for most of the tested operating range. For the IMEP higher than 4.5 bar, there is a significant increase attributed to the lower air excess factor, late injection and combustion, which leads to freezing CO oxidation chemistry. It is important to note that for injection pressure of 50 bars, when a more optimal fuel injection strategy can be realized, CO emissions remained below 5 g/kWh up to an IMEP of 5.4 bar. The obtained results show that the engine operating with MSR reformate leads to a reduction in CO emissions by 70–97% in the entire tested range of

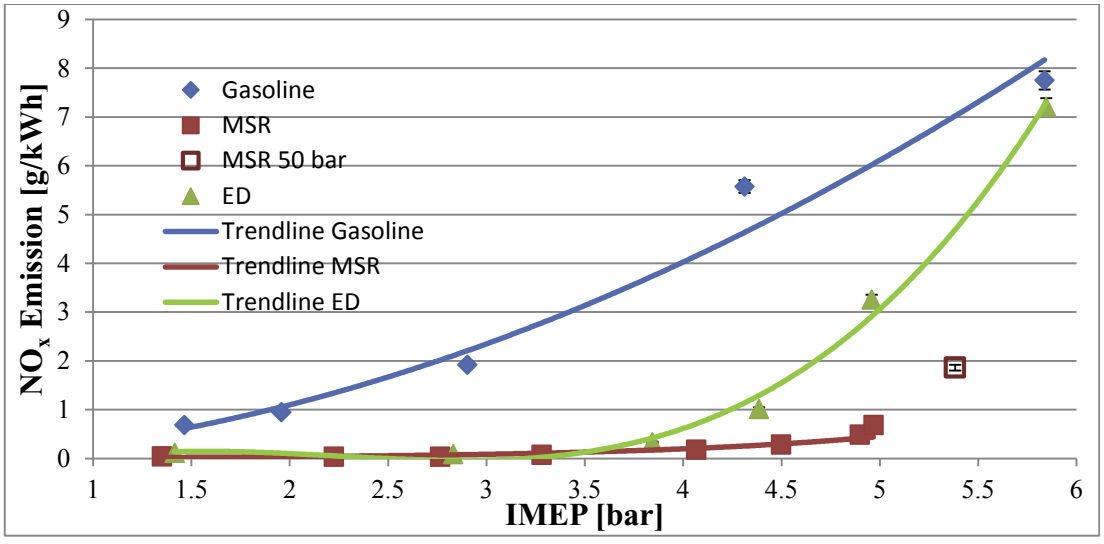

Fig. 8. NO_x emission for gasoline, ED and MSR products as function of IMEP. Engine speed 2800 rpm; ED and MSR at WOT; injection pressure at 40 bar; injection start at 230 CAD. The ignition timing for gasoline, MSR and ED was constant at 333, 347 and 339 CAD, respectively. The error bars show uncertainty for the calculated NO_x emission values.

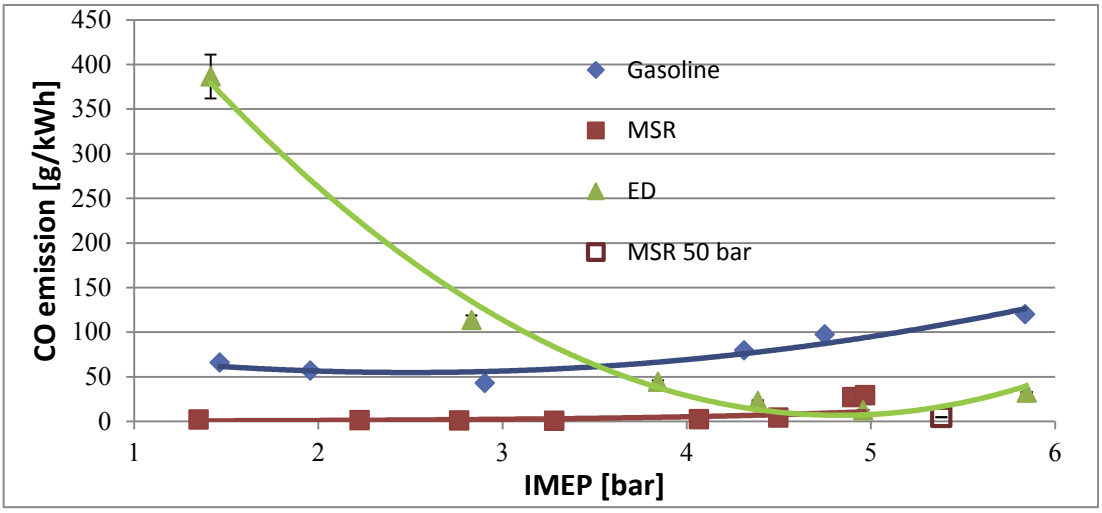

Fig. 9. CO emission for gasoline, ED and MSR products as function of IMEP. Engine speed 2800 rpm; ED and MSR at WOT; injection pressure at 40 bar; injection start at 230 CAD. The ignition timing for gasoline, MSR and ED was constant at 333, 347 and 339 CAD, respectively. The error bars show uncertainty for the calculated CO emission values.

engine loads. The high CO emissions for the case of gasoline are influenced, of course, by the fuel supply method (carburetor). The reason for the significant CO emission increase at low loads in case of engine feeding with ED products is the work with WOT (at high λ values up to 2.7), which resulted in the poor and incomplete combustion of the ED reformate fuel (Fig. 7). This problem is clearly reflected in the high level of HC emissions when the ICE is fed with ED products operating unthrottled at low-load regimes (Fig. 10).

As seen from Fig. 10, the HC emissions of the engine fed by MSR products are extremely low because the only source of HC formation in this case is lubricating oil. For gasoline, the emissions are higher as a result of combustion of the much richer mixture created in the carburetor compared to the reformate fuels. ICE operating with MSR products leads to a reduction in HC emissions by 85–97% in the entire tested range of engine loads. The extremely high HC emissions at low loads in the case of engine feeding with ED reformate are due to the poor combustion efficiency, as explained above (Fig. 7). The incomplete combustion of ED reformate at low loads is also misleading when CO_2 emissions are considered. As seen from Fig. 11, CO_2 emissions of the engine fed with ED reformate seem to be beneficially low, but this is only because a high percentage of carbon introduced to the cylinder with the fuel is emitted as HC or CO (Figs. 7, 9 and 10).

Even though our testing procedure did not exactly meet the requirements of the EPA standard CFR-40 part 1054 for non-handheld engines, we have performed a comparison with the standard limits, as shown in Table 4, for the purpose of relative assessment of the engine performance when fed by gasoline and MSR products.

As seen from Table 4, the emissions of the baseline ICE fed with gasoline exceed the standard limits, whereas in case of engine feeding with MSR products, it emits almost an order of magnitude

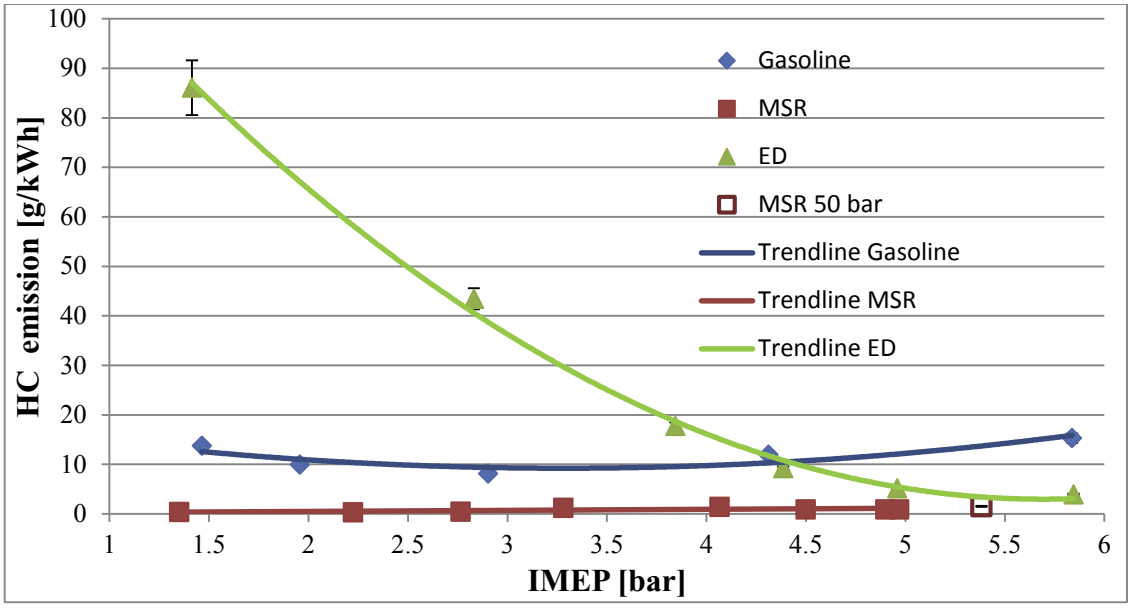

Fig. 10. HC emission for gasoline; ED and MSR products as functions of IMEP. Engine speed 2800 rpm; ED and MSR at WOT; injection pressure at 40 bar; injection start at 230 CAD. The ignition timing for gasoline, MSR and ED was constant at 333, 347 and 339 CAD, respectively. The error bars show uncertainty for the calculated HC emission values.

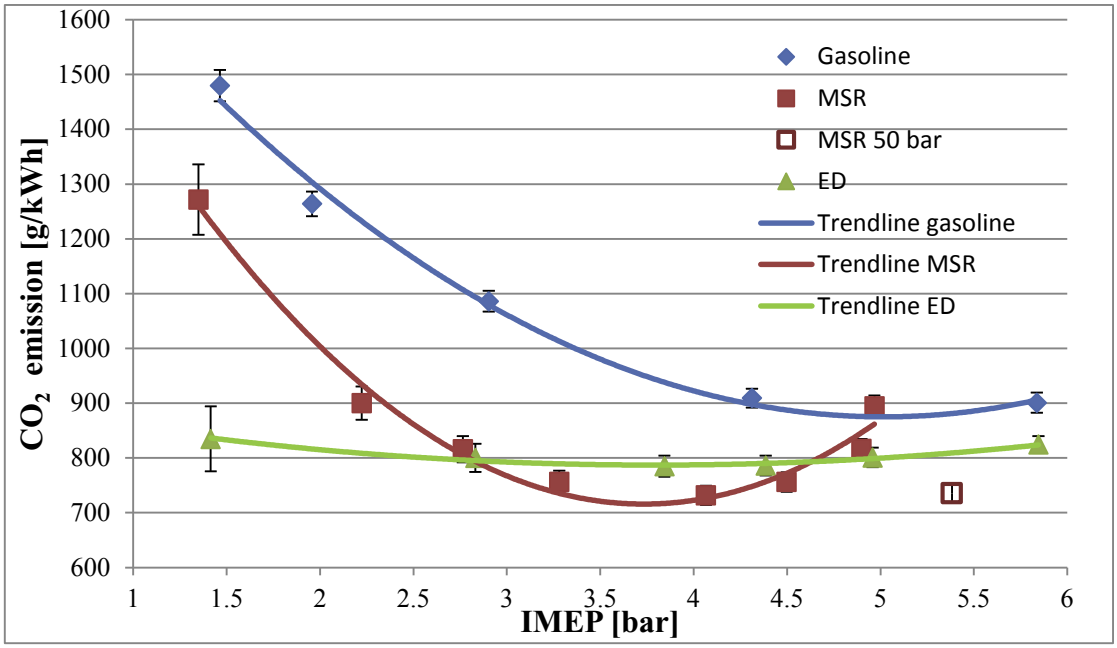

Fig. 11. CO_2 emissions for gasoline, ED and MSR products as a function of IMEP. Engine speed 2800 rpm; ED and MSR at WOT; injection pressure at 40 bar; injection start at 230 CAD. The ignition timing for gasoline, MSR and ED was constant at 333, 347 and 339 CAD, respectively. The error bars show uncertainty in the calculated CO_2 emission values.

Table 4
Comparison of emissions calculated according to CFR-40 part 1054 phase 3 (class I engines) based on maximum IMEP 5.4 bar for the ICE fed with gasoline and MSR products.

	MSR	Gasoline	Standard limits
NO_x + HC [g/kWh]	1.1	13.5	10
CO [g/kWh]	3.5	67	610 (5 for marine generator engines)

less NO_x + HC emissions than the regulation prescribes. The obtained results give an indication of the good potential of MSR-fed ICE in achieving a substantial reduction of pollutant emissions. However, because the experiments reported in this article were conducted with a low compression ratio engine (meaning low efficiency, but also low temperature and NO_x formation) at constant speed and ignition timing, it is too early to indicate whether there will be a need for exhaust gas aftertreatment in the case of MSR-fed ICE at an automotive scale.

CO_2 emissions, in the cases of engine feeding with reforming products, are lower compared to gasoline in most of the operating range thanks to the increased efficiency and low carbon intensity of the alcohol primary fuels. The only exception is at the highest IMEP regime for MSR, and this is due to the reduced efficiency caused by the late end of injection that was necessary to achieve the required power at an injection pressure of 40 bars. When the injection pressure was raised to 50 bar, the CO_2 emission was reduced substantially to 735 g/kWh at IMEP of 5.4 bar as a result of the engine efficiency improvement. For comparison purposes, CO_2 emissions at the same IMEP when the engine was fed with gasoline were measured to be approximately 900 g/kWh (Fig. 11).

The particle number (PN) emissions proved to be much harder to assess. We did not find any clear relationship between engine operating regime and PN emissions. Even for the same operating regime, the measured PN concentrations were extremely unstable, showing different types of behavior. Fig. 12 shows an example of two measurements taken for the same operating mode.

It is possible to distinguish a number of different patterns from the observed PN emission behavior. The red line shows a case where low PN concentrations were measured most of the time with a single sharp spike where the PN level rises above the baseline level by more than two orders of magnitude. The green line demonstrates the multiple-spike behavior of PN emissions. Measurements with low PN concentrations (close to 10^5 cm^{-3}) that are stable along the 2–3 min measurement period were recorded as well. Similar behavior in measured PN concentrations was reported previously for an SI engine [36]. The authors of this publication related these spikes to combustion chamber deposit breakup. In our measurements, the baseline level of the measured PN concentrations was found to be in the range of 10^5–10^6 cm^{-3}, which is close to the PN concentrations observed for a hydrogen-fueled engine where lubrication oil was the only reason for PN formation [37]. We suppose that in our case, the main sources of PN emissions are both the breakup of combustion chamber deposits and lubricant combustion. Further research is required to better understand the mechanism and physical reasons for the observed phenomena.

4. Summary and conclusions

An experimental setup — based on a single-cylinder SI ICE with the ability to operate as a DI engine fed by gaseous fuels — was built. It was used to conduct experiments with two of the most widely investigated alcohol reforming schemes, which include low temperature ethanol decomposition and methanol steam reforming products as well as gasoline (as a reference case).

It was shown that for both studied reformate types, the engine can work unthrottled up to idle, but at the expense of an increased COV, reduced combustion and indicated efficiency. The problems of combustion efficiency and cycle-to-cycle variability and the consequent efficiency reduction were much more severe with the ED reformate because of the smaller hydrogen content in the mixture. COV values, in the case of engine feeding with the MSR reformate, did not exceed 0.05 up to $\lambda = 3.5$. Engine feeding with the MSR reformate resulted in much higher heat release rates,

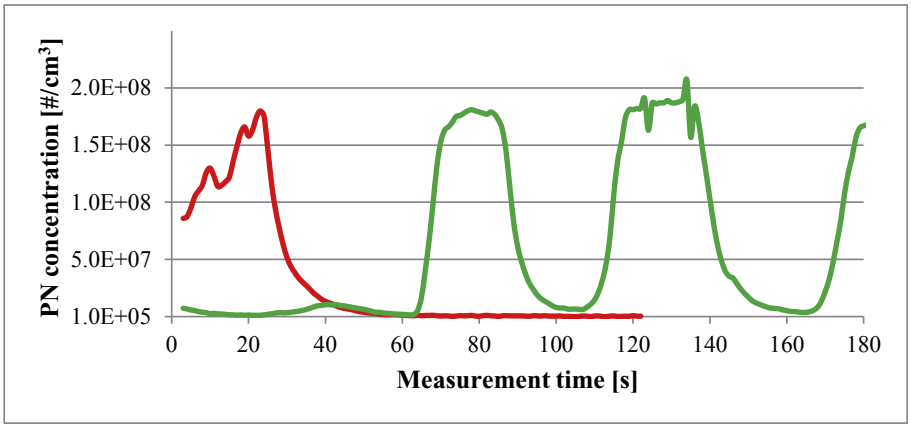

Fig. 12. Total PN concentrations. Engine speed 2800 rpm; MSR products at WOT; $\lambda = 2.5$; measured power, 850 W; injection pressure at 40 bar.

which is reflected in substantially shorter flame development angles (13–15 deg.) compared to gasoline (30 deg.) or methane (29 deg.).

The thermal efficiency of the engine fueled by MSR products was improved by 18–39% compared to the engine operating with gasoline. The results of the experiments showed that with the current gaseous direct injector (flow area of 0.85 mm^2), injection pressure of 40 bar is insufficient to achieve IMEP pressures higher than 4.5 bar with high efficiency. An option of increasing the injector flow area or the injection pressure should be considered and analyzed. This, in turn, may require an increase of the reforming pressure.

The MSR reformate showed much lower pollutant emissions compared to ED products and gasoline. Engine feeding with MSR resulted in emissions reductions of 73–94%, 90–96%, 85–97%, and 10–25% in NO_x, CO, HC and CO_2 emissions, respectively, compared to gasoline feeding.

Overall, the reformate fuels have showed great improvement over gasoline in terms of combustion behavior, such as reduced COV for a wide range of excess air ratios and a faster heat release rate. These fundamental benefits are reflected in a significant improvement of engine thermal efficiency and a dramatic reduction in pollutant emissions. It is expected that further improvement can be achieved if ignition timing, throttling and injector positioning & orientation are optimized. The potential of meeting future emission legislation without a need for exhaust gas aftertreatment should be explored. ED has an advantage over MSR in terms of primary fuel energy density, reformate energy density and required heat transfer area for the reformer but has major disadvantages in thermal efficiency and pollutant emissions. Both schemes show good prospects for further development.

Acknowledgements

The authors gratefully acknowledge the financial support of the Israel Science Foundation (grant 1728/12); Israel Ministry of Environmental Protection (grant 133-1-5); Israel Ministry of National Infrastructures, Energy and Water Resources (grant 215-11-025); Israel Ministry of Science, Technology and Space; Wolfson Family Charitable Trust; Rieger Foundation and the Grand Technion Energy Program.

References

[1] Wang Z, Liu H, Long Y, Wang J, He X. Comparative study on alcohols–gasoline and gasoline–alcohols dual-fuel spark ignition (DFSI) combustion for high load extension and high fuel efficiency. Energy 2015;82:395–405.
[2] Wang X, Ge Y, Zhang C, Tan J, Hao L, Liu J, et al. Effects of engine misfire on regulated, unregulated emissions from a methanol-fueled vehicle and its ozone forming potential. Appl Energy 2016;177:187–95.
[3] Sá S, Silva H, Brandão L, Sousa JM, Mendes A. Catalysts for methanol steam reforming—a review. Appl Catal B Environ 2010;99:43–57.
[4] Lorenzut B, Montini T, De Rogatis L, Canton P, Benedetti A, Fornasiero P. Hydrogen production through alcohol steam reforming on Cu/ZnO based catalysts. Appl Catal B Environ 2011;101(3–4):397–408.
[5] He M, Zhang X, Zeng K, Gao K. A combined thermodynamic cycle used for waste heat recovery of internal combustion engine. Energy 2011;36(12):6821–9.
[6] Shu G, Zhao M, Tian H, Wei H, Liang X, Huo Y, et al. Experimental investigation on thermal OS/ORC (Oil storage/organic Rankine Cycle) system for waste heat recovery from diesel engine. Energy 2016;107:693–706.
[7] Chakravarthy VK, Daw CS, Pihl JA, Conklin JC. Study of the theoretical potential of thermochemical exhaust heat recuperation for internal combustion engines. Energy Fuels 2010;24(3):1529–37.
[8] Verhelst S. Recent progress in the use of hydrogen as a fuel for internal combustion engines. Int J Hydrogen Energy 2014;39:1071–85.
[9] Verhelst S, Wallner T. Hydrogen-fueled internal combustion engines. Prog Energy Combust Sci 2009;35:490–527.
[10] Morgenstern DA, Fornango JP. Low-temperature reforming of ethanol over copper-plated raney nickel: a new route to sustainable hydrogen for transportation. Energy Fuels 2005;19:1708–16.
[11] Wheeler JC, Stein RA, Morgenstern DA, Sall ED, Taylor JW. Low-temperature ethanol reforming: a multi-cylinder engine demonstration. 2011. SAE Technical Paper No. 2011-01-0142.
[12] Liao CH, Horng RF. Investigation on the hydrogen production by methanol steam reforming with engine exhaust heat recovery strategy. Int J Hydrogen Energy 2016;41(9):4957–68.
[13] Wijaya WY. Methanol steam reforming for hydrogen production: concept and evaluation of integrated advanced energy system. PhD Thesis. Tokyo, Japan: Tokyo Institute of Technology; 2013. p. 102.
[14] Twigg MV, Spencer MS. Deactivation of copper metal catalysts for methanol decomposition, methanol steam reforming and methanol synthesis. Top Catal 2003;22(3–4):191–203.
[15] Cao W, Chen G, Li S, Yuan Q. Methanol-steam reforming over a ZnO–Cr2O3/CeO2–ZrO2/Al2O3 catalyst. Chem Eng J 2006;119:93–8.
[16] Marbán G, López A, López I, Valdés-Solís T. A highly active, selective and stable copper/cobalt-structured nanocatalyst for methanol decomposition. Appl Catal B Environ 2010;99(1):257–64.
[17] Pettersson L, Sjostrom K. Decomposed methanol as a fuel—a review. Combust Sci Technol 1991;80(4–6):265–303.
[18] Matthias NS, Wallner T, Scarcelli R. A hydrogen direct injection engine concept that exceeds US DOE light-duty efficiency targets. SAE Int J Engines 2012;5:838–49.
[19] Hagos FY, Aziz ARA, Sulaiman SA. Syngas (H_2/CO) in a spark-ignition direct-injection engine. Part 1: combustion, performance and emissions comparison with CNG. Int J Hydrogen Energy 2014;39:17884–95.
[20] Hagos FY, Aziz ARA, Sulaiman SA. Investigation of deposit formation in direct-injection spark-ignition engine powered on syngas. Int J Automot Technol 2015;16(3):479–85.
[21] Li G, Zhang Z, You F, Pan Z, Zhang X, Dong J, et al. A novel strategy for hydrous-ethanol utilization: demonstration of a spark-ignition engine fueled with hydrogen-rich fuel from an onboard ethanol/steam reformer. Int J Hydrogen Energy 2013;38(14):5936–48.
[22] Shimada A, Ishikawa T. Improved thermal efficiency using hydrous ethanol reforming in SI engine. 2013. SAE Technical Paper No. 2013-24-0118.
[23] Yoon HC, Otero J, Erickson PA. Reactor design limitations for the steam reforming of methanol. Appl Catal B Environ 2007;75(3):264–71.

[24] He Z, Gao Z, Zhu L, Li S, Li A, Zhang W, et al. Effects of H_2 and CO enrichment on the combustion, emission and performance characteristics of spark ignition natural gas engine. Fuel 2016;183:230–7.
[25] Tartakovsky L, Baibikov V, Veinblat M. Comparative performance analysis of SI engine fed by ethanol and methanol reforming products. 2013. SAE Technical Paper No. 2013-01-2617.
[26] Poran A, Tartakovsky L. Energy efficiency of a direct-injection internal combustion engine with high-pressure methanol steam reforming. Energy 2015;88:506–14.
[27] Peppley BA, Amphlett JC, Kearns LM, Mann RF, Roberge PR. Hydrogen generation for fuel-cell power systems by high-pressure catalytic methanol-steam reforming. In: Energy conversion engineering conference, 1997. IECEC-97, proceedings of the 32nd intersociety. IEEE; 1997, July. p. 831–6.
[28] Tartakovsky L, Amiel R, Baibikov V, Fleischman R, Gutman M, Poran A, et al. SI engine with direct injection of methanol reforming products–first experimental results. 2015. SAE Technical Paper No. 2015-32-0712.
[29] Wang X, Grose MA, Caldow R, Osmondson BL, Swanson JJ, Chow JC, et al. Improvement of Engine Exhaust Particle Sizer (EEPS) size distribution measurement–II. Engine exhaust particles. J Aerosol Sci 2016;92:83–94.
[30] Heywood JB. Internal combustion engine fundamentals. New York: McGraw-Hill; 1988.
[31] Lee K, Yoon M, Sunwoo M. A study on pegging methods for noisy cylinder pressure signal. Control Eng Pract 2008;16(8):922–9.
[32] Shavit A, Gutfinger C. Thermodynamics: from concepts to applications. Boca Raton: CRC Press; 2008.
[33] Moffat RJ. Describing the uncertainties in experimental results. Exp Therm fluid Sci 1988;1(1):3–17.
[34] Brunt MF, Pond CR. Evaluation of techniques for absolute cylinder pressure correction. 1997. SAE Technical Paper No. 970036.
[35] Omari A, Shapiro M, Tartakovsky L. Laminar burning velocity of alcohol steam reforming products and effects of cellularity on flame propagation. 2015. SAE Technical Paper No. 2015-01-0775.
[36] Graskow BR, Kittelson DB, Abdul-Khalek IS, Ahmadi MR, Morris JE. Characterization of exhaust particulate emissions from a spark ignition engine. 1998. SAE Technical Paper No. 980528.
[37] Miller AL, Stipe CB, Habjan MC, Ahlstrand GG. Role of lubrication oil in particulate emissions from a hydrogen-powered internal combustion engine. Environ Sci Technol 2007;41(19):6828–35.